# *Monitoring rice crop and yield estimation with Sentinel-2 data*

Jesús SORIANO-GONZÁLEZ[1, 2], Eduard ANGELATS[1, †], Maite MARTÍNEZ-EIXARCH[2], Carles ALCARAZ[2, *]

[1] *Division of Geomatics, Centre Tecnològic de Telecomunicacions de Catalunya (CTTC/CERCA), Av. Gauss 7, E-08860 Castelldefels, Barcelona, Spain*

[2] *IRTA Marine and Continental Waters, Carretera Poble Nou Km 5.5, E-43540 Sant Carles de la Ràpita, Tarragona, Spain*

*Corresponding author: carles.alcaraz@irta.cat // carles.alcaraz@gmail.com

[†]Co-corresponding author: eduard.angelats@cttc.cat

## Graphical abstract

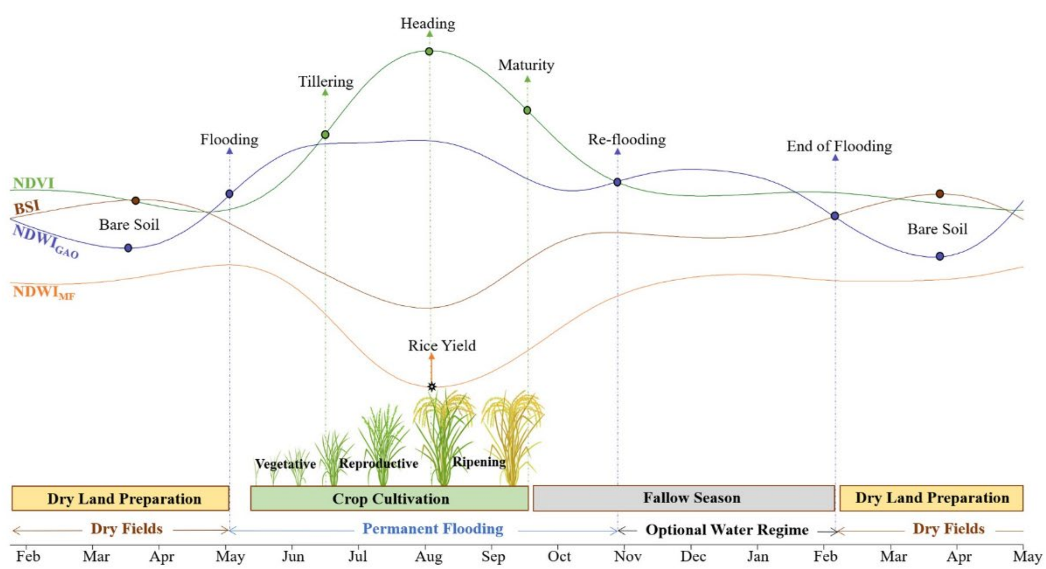

## Abstract

The future success of rice farming will lie in developing productive, sustainable, and resilient farming systems in relation to coexistent ecosystems. Thus, accurate information on agricultural practices and grain yield at optimum temporal and spatial scales is crucial. This study evaluates the potential application of Sentinel-2 (S2) to monitor the dynamics of rice fields in two consecutive seasons (2018 and 2019) in the Ebro Delta growing area. For this purpose, time series of four different spectral indexes (NDVI, $NDWI_{MF}$, $NDWI_{GAO}$, and BSI), derived from smoothed S2 data at 20 m spatial resolution, were generated. Then, a combination of the first and second derivative analysis on the temporal profiles of spectral indexes was used to automatically identify key phenology and management features from regional to field scale; and for estimating crop yield at fields. Features extracted from NDVI and $NDWI_{GAO}$ were used for identifying significant phenological stage dates (*i.e.* Tillering, Heading Date, and Maturity), and field status (*i.e.* hydroperiod), although the performance of the proposed method at field-scale was limited by S2 data gaps. The absolute minimum of $NDWI_{MF}$ showed great potential for estimating rice yield, including different cultivars ($r$ = - 0.8), and less sensibility to the number of valid images. Sentinel-2 alone cannot assure a consistent phenology monitoring at all fields but demonstrated strong capabilities for studying the performance of rice fields, thus must be considered in the development of new strategies for the management of rice-growing areas.

**Keywords:** Remote sensing, Agriculture; Time series; Smoothing; Rice phases; Ebro Delta

## 1. Introduction

Rice provides food for more than half of the world's population, occupying more than 12 % of the world crop area, providing important ecosystems services such as habitat for fauna, prevention of saline intrusion and soil erosion, subsidence mitigation, and nutrient cycling (Tornos *et al*., 2015). Accurate information on crop practices (*e.g.* water management, hydroperiod, crop performance) along space and time is crucial for planning agricultural and environmental policies (Mosleh et al., 2015). However, vegetation dynamics and hence rice yield, vary temporally and spatially due to several factors such as differences in soil properties, climatology, and management practices (Casanova, 1998; Bradley *et al.*, 2007). Thus increasing the difficulty to assess the spatial variability of the agricultural practices through field surveys, which is also costly and time-consuming. Sometimes, the only available information comes from farmer's declarations (Courault et al., 2020). With the rapid development of geospatial technology in the last years, the acquisition of high-quality spatial and temporal data has become cost-effective and efficient, offering opportunities for land monitoring and management. In particular, multispectral satellite remote sensing has proved its usefulness in monitoring rice crops, water regime, and in estimating yield production (Mosleh *et* al., 2015; Dong and Xiao, 2016). Usually, spectral indices (SI) are used as a proxy for vegetation, flooding regime, and crop efficiency because they integrate the information of two or more spectral bands which are sensitive to different plant or soil characteristics (*e.g.* plant pigments or water content) (Zeng *et al.*, 2020). Coarse-resolution sensors such as MODIS, AVHRR, SPOT-VEGETATION, and MERIS have been widely used since high-quality datasets are readily available and easier to process (Bolton et al., 2020, Zhu et al., 2019). However, because their coarse spatial resolutions (from 250 m) is difficult to differentiate management practices at single-field level (Liu et al., 2020).

Therefore, remote sensing data with better spatial resolution is preferred; for instance, Landsat is able to provide images up to 30 m but at low temporal resolution (16 days) which is still an important constraint (Fernández-Beltrán et al., 2021).

The Sentinel-2 (S2) satellite constellation is an Earth observation mission launched by the European Spatial Agency (ESA) under the Copernicus programme to provide accurate, timely, and easily accessible information of the land surface, with improved capabilities for vegetation mapping and monitoring, and phenology estimation (reviewed in Misra *et al*., 2020). The S2 senses at 13 different spectral bands (ranging from 443 nm to 2190 nm), including visible (VIS), near-infrared (NIR), and shortwave infrared (SWIR), at spatial resolutions of 10 m, 20 m, and 60 m (depending on the band), with a revisiting time of 5 to 10 days. However, the use of S2 still presents some limitations related to time series development, including noise and data gaps (*e.g.* atmospheric correction errors, decreased reflectance by shadows, cloud presence). In this sense, a common practice with multispectral remote sensing data is the usage of multi-temporal images composites derived from the combination of best quality pixels from images within a defined period (Sakamoto *et al.*, 2005; Wang *et al.*, 2012; Tornos *et al.*, 2015). Nevertheless, finding noise-free values may be complicated for short periods of time, and increasing the compositing period may lead to the loss of information (Zeng *et al.*, 2020). In some cases, there is insufficient cloud-free information present in the multi-temporal data to compose a cloud-free image (Schmitt *et al.*, 2019), and it is necessary to smooth data by filter-based methods or function fitting methods to fill temporal gaps and minimize the residual noise (Bradley *et al.*, 2007; Geng *et al.*, 2014). A complementary approach is the integration of data from different platforms (*e.g.* Landsat, Sentinel-2), to reduce temporal gaps in multi-temporal composites (Liu et al., 2020).

However, data-fusion complexities (*i.e.* temporal gaps, spectral harmonization, heterogeneity in cloud-masking methods, and spatial registration) make the possibility of using single-platform remote sensing data very attractive.

After completing the spectral index (SI) time series, the analysis of vegetation phenology, irrigation regime, and crop yield estimation will depend on the ability to characterize intra- and inter-annual dynamics at optimal scales. For the monitoring of rice-growing areas, it is crucial to differentiate key phenological stages (*e.g.* heading date, maturity) and management practices (*e.g.* flooding, harvest), both in space and time, particularly at small spatial scales. The main aim of this study is to assess the capability of Sentinel-2 to monitor rice crops in a Mediterranean growing area. Specific objectives are (i) to generate cloud-free spatiotemporal time series of four SI (NDVI, NDWIMF, $NDWI_{GAO}$, and BSI) along two consecutive crop seasons (2018 and 2019), (ii) to automatically identify the main phenological stages and management practices at different scales (from regional to field), and (iii) to provide estimates of rice yield.

## 2. Materials and methods

### 2.1. Study area

The Ebro River (NE Iberian Peninsula) is one of the most important tributaries of the Mediterranean Sea, it is 910 km long, has a drainage area of 85,362 $km^2$, and a mean annual flow of 426 $m^3 \cdot s^{-1}$ (Genua-Olmedo *et al.*, 2016). The Ebro Delta (Fig. 1), with an extension of *ca*. 32,500 ha, contains a number of ecosystems with high ecological value (*e.g.* wetlands, coastal lagoons, and fresh water springs) included in the Natura 2000 network of the European Union and protected as Natural Park and UNESCO Biosphere Reserve. The 65 % of the delta area (21,125 ha) is devoted to rice farming (Fig. 1), constituting the main economic activity in the region and providing important ecosystems services. The climate is typically Mediterranean with a mean annual precipitation of about 500 mm, mostly distributed during spring and autumn, and a mean annual temperature of 18 ˚C with mild winters (mean temperature in January is 9 ˚C) and hot summers (mean temperature in July is 24 ˚C).

In the Ebro Delta, rice is grown from late April to September and left fallow during the rest of the year (Fig. 2). In the growing season, water management consists of permanent flooding from sowing time (late April-early May) to two weeks before harvest (September), the water layer is *ca*. 5-15 cm deep. During the vegetative and early reproductive stages, short draining periods can occur for either facilitating early crop establishment, or for herbicide and fertilizer applications. After harvest, fields are re-inundated for the incorporation of rice straw into the soil. Thereafter fields are either flooded from October to December (Re-flooding) or left to progressively drain according to farmers' practices. From January to March rice fields are left dry for soil labor operations (harrowing and fertilizer application) and flooded in Mid-April, at the beginning of the next cultivation period (Martínez-Eixarch *et al.*, 2018). The cultivars grown in the Ebro Delta, are japonica-type with medium grain size and growth cycle of *ca*. 120 to 140 days from sowing to maturity. In general, the variability of cultivars grown in the area within a year is low, *ca*. 5 different rice cultivars cover most of the cultivation area.

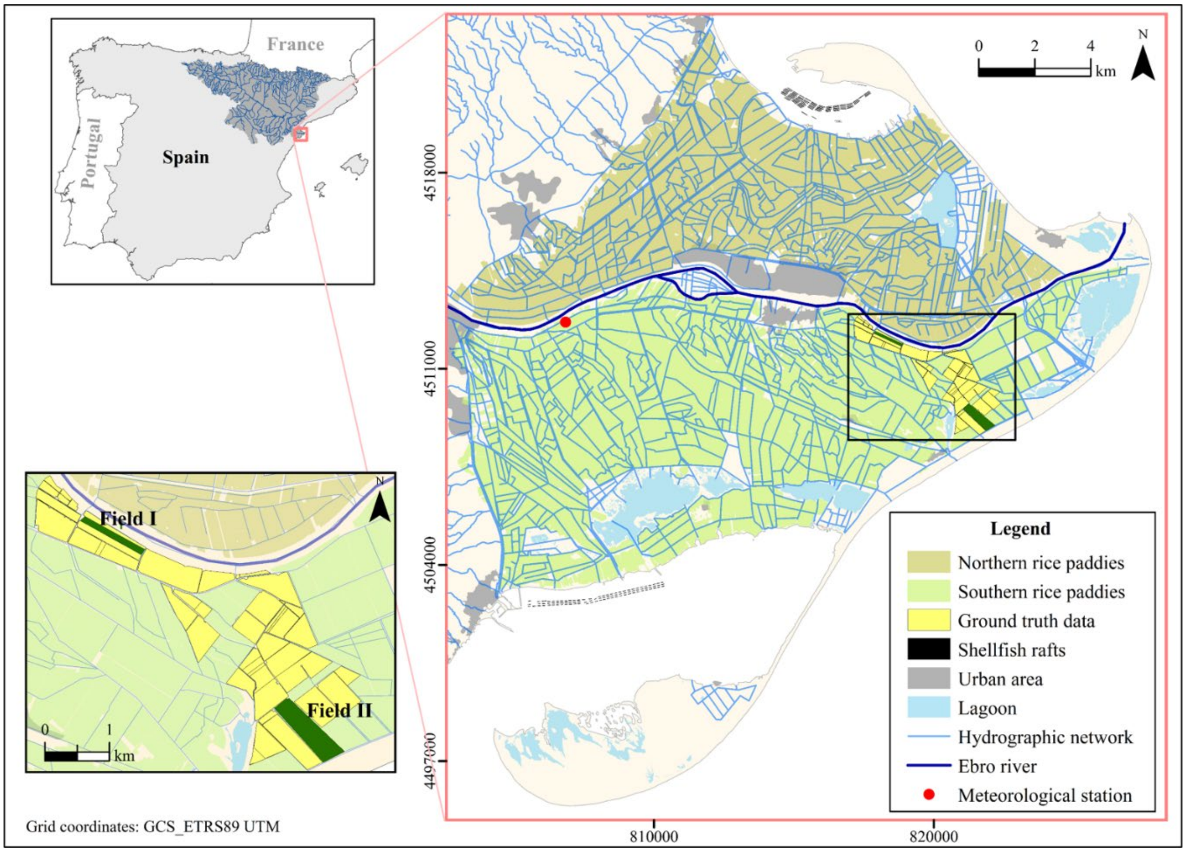


**Figure 1.** Location of the Ebro Delta and coverage of rice paddies under study. Fields I and II are used in support of sections 3 and 4.

## 2.2. Study design

The study was carried out over two consecutive years (2018-2019). Annual cadastral data of all rice parcels were obtained from the Department of Agriculture, Livestock, fisheries, and food of the regional government (http://agricultura.gencat.cat). Four scenarios, considering different spatial scales, were analyzed: Scenario 'A' included all rice fields in the Ebro Delta; Scenario 'B' and 'C' considered all paddies in the northern and southern hemidelta, respectively; and in Scenario 'D' 67 subsets of rice fields were analyzed (Fig. 1) for which field and crop information, including at least cultivar, agricultural practices (*i.e.* sowing, harvesting dates), or yield ($kg \cdot ha^{-1}$), were obtained from the owner. In Scenario

'D', Field I and Field II (Fig. 1) were chosen as an example to facilitate results interpretation. Field I (10.8 ha) is close to the Ebro River (Fig. 1) and seeded with *Mare* cultivar in both 2018 and 2019. Field II is the largest field in scenario 'D' (37.4 ha), *Bomba* and *Sirio* cultivars were grown in 2018 and 2019, respectively.

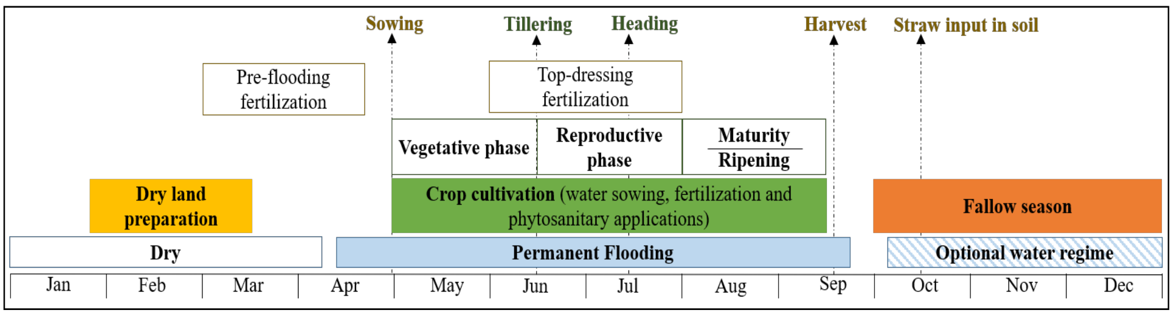


**Figure 2.** Rice farming calendar in the Ebro Delta. Adapted from (Martínez-Eixarch et al., 2018)

### 2.3. Satellite data

Google Earth Engine (GEE), a cloud-based platform for long-term geospatial analysis (Gorelick *et al.*, 2017), was used for data access, clouds and clouds shadows detection, image pre-processing (*i.e.* image subset, mosaicking of tiles and image resampling), and spectral index calculation. In GEE, image collections of both Sentinel-2 A/B (S2) top of atmosphere (L1C, TOA) and atmospherically corrected for surface reflectance (L2A, BOA) from 1$^{st}$ of January 2018 to the 31$^{st}$ of December 2019 were used. All images were obtained from the same orbit (051) and tiles (TCF31 and TBF31) to homogenize remote sensing measurements and ensure the full coverage of the study area. First, all available BOA images within the study period were loaded ($N_{images}$ = 138); then, TOA images were selected based on the available BOA dates. TOA images were needed as the base of the method used for masking clouds and cloud shadows (adapted from Schmitt *et al.*, 2019). Water masking was not applied to avoid interferences with flooded rice paddies and, only the second module of the Schmitt *et al.* (2019) method was used (*i.e.* image quality score module). This generates a pixel scoring for each independent TOA image and date by combining the probabilities of cloud presence given different assumptions about brightness, moisture, and snow. Cloud masks were derived with a threshold of 0.3 on the pixel score. Then, the cloud masks, in conjunction with the TOA images metadata (sun azimuth and zenith) and a range of possible cloud heights (from 200 m to 10000 m) were used to generate shadow scores images and shadow masks. The threshold on the sum of infrared bands to include as possible shadows was lowered from 0.3 (default) to 0.1 for reducing the miss-classification of flooded paddies. For more detailed information on the cloud and shadow masking method see Schmitt *el al*. (2019).

The computed masks for TOA images were applied to the BOA collection, and after clouds and clouds shadows masking, S2 BOA images were cropped to the region of interest (Fig. 1), daily mosaicked (merging of same-date tiles), and resampled to 20 m spatial resolution. For each scenario images were filtered according to cloud and shadow mask percent coverage over rice fields. Only those images with at least 80 % of valid pixels per scenario were included in the posterior analysis and, for each valid S2 image (Fig. 3) SI were computed (see section 2.4) at pixel level (*i.e.* 20 m x 20 m) and then averaged at different scenarios scales.

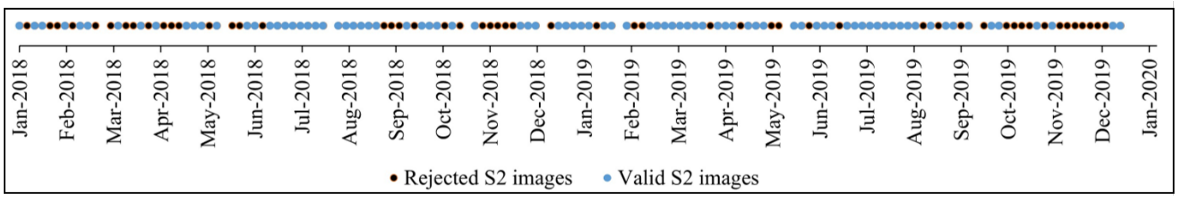


**Figure 3.** Valid and rejected S2 images

### 2.4. Spectral indices

Four SI were calculated according to their utility in estimating rice development, water management, or production (Table 1). These two and three-band normalized difference indices are dimensionless, range between -1 and 1, and exploit the VIS, NIR, and SWIR regions of the spectrum (Table 1). The Normalized Difference Vegetation Index (NDVI) exploits the chlorophyll light absorption in the VIS-red region of the spectrum and the high reflectance of vegetation in the NIR (Rouse *et al.*, 1974). The Normalized Difference Water Index proposed by McFeeters (1996), here referred to as $NDWI_{MF}$, was developed for delineating open water bodies by making use of the NIR and VIS-green light. The Normalized Difference Water Index by Gao (1996), here referred to as $NDWI_{GAO}$, was developed for the remote sensing of vegetation liquid water by using the NIR and SWIR channels. The Bare Soil Index (BSI) is used to identify bare soil areas and fallow lands, by combining information from the VIS-blue, VIS-red, NIR, and SWIR channels (Rikimaru *et al.*, 2002).

**Table 1.** SI used in this study. The R(λ) in equations stands for Surface Reflectance at S2 band with centered wavelength λ in nm*.

| Spectral Index | Equation |
|---|---|

| | |
|---|---|
| Normalized Difference Vegetation Index - NDVI (Rouse et al. 1974) | $\frac{R(842) - R(665)}{R(842) + R(665)}$ |
| Normalized Difference Water Index - $NDWI_{GAO}$ (Gao et al., 1996) | $\frac{R(842) - R(1610)}{R(842) + R(1610)}$ |
| Normalized Difference Water Index – $NDWI_{MF}$ (McFeeters et al., 1996) | $\frac{\mathrm{R}(560) - \mathrm{R}(842)}{\mathrm{R}(560) + \mathrm{R}(842)}$ |
| Bare soil index - BSI (Rikimaru et al., 2002) | $\frac{(\mathrm{R}(1610) + \mathrm{R}(665)) - (\mathrm{R}(842) + \mathrm{R}(490))}{(\mathrm{R}(1610) + \mathrm{R}(665)) + ((842) + \mathrm{R}(490))}$ |

* R(λ) – S2 bands: R(490) - B2, R(560) – B3, R(665) – B4, R(842) – B8, R(1610) – B11 and R(2190) – B12.

## 2.5. Data smoothing

For each S2 valid image and considered scenario, SI data were smoothed with a cubic spline fitting method, thus estimating daily data at different scenario scales, and reducing multi-factorial noise in the original data (*e.g.* atmospheric correction or cloud/shadows miss-detection derived errors). Cubic spline fitting is based on the minimization of quadratic errors with curvature type regularization by joining piecewise polynomials smoothly at selected knots from the original data points (Wang, 2011). Thus, the fit is not limited by any method-constrained shape, but phenological shape is driven entirely by the data (Bradley *et al.*, 2007). The cubic spline smoothing was done in R version 3.6 (R Core Team, 2017) by using the *smooth.spline* function; all data were included as possible knots and the *spar* smoothing parameter was fixed to 0.65.

## 2.6. Rice phenology, hydroperiod and yield

Smoothed NDVI and $NDWI_{GAO}$ time series were combined to assess rice phenology, crop evolution, and flooding practices. The BSI was computed as an additional state indicator complementing the analysis of NDVI and $NDWI_{GAO}$, but it was not included in the feature extraction system. The $NDWI_{MF}$ was only used for crop yield estimates. The method for automatic extraction of key features consisted on the assumption that the presence of local maximums, minimums, and critical points (inflection points) in spectral index trends is related to changes in soil, flooding, or vegetation stages (Zheng et al., 2016 and Liu et al., 2017). For the different scenarios considered, SI time series were smoothed, and all minimums and maximums were identified from the first derivative analysis; and all possible inflection points were identified for NDVI, $NDWI_{GAO}$ and BSI. Then, local and critical points of interest were selected (Table 2).

First, the absolute maximum NDVI was associated with the middle heading date (HD) of each growing season as proposed in (Wang et al., 2014; Tornos et al., 2015; Zhang et al., 2019). From the HD, other key features were derived for each year following the identification steps and order presented (Table 2 and Fig. 4). The order was based on the expected occurrence of events (*e.g.* Active tillering occurs before HD; End of flooding of one growing season occurs before flooding of the following one), allowing to automatize the process by avoiding unwanted minimum/maximum and inflection points. Key features related with rice status were extracted first from NDVI, and then $NDWI_{GAO}$ was used to assess water management (Table 2 and Fig. 4).

**Table 2**. Key phenological and field-status features identified in this study.

| Acronym | Key feature | Description | Identification |
|---|---|---|---|
| HD | Heading Date | Phenology: Vegetative development of rice is maximum. | Absolute maximum NDVI |
| T | Tillering | Phenology: Active tillering. The number of leaves increases rapidly | First inflection point of NDVI before HD |
| M | Maturity | Phenology and Management: Close to end of maturation stage | First inflection point of NDVI after HD |
| F | Flooding | Management: Flooding of rice fields have started | First inflection point of $NDWI_{GAO}$ before T. It must be after minimum $NDWI_{GAO}$ |
| EF | End of Flooding | Management: Water in fields is emptied before the land preparation | First inflection point of $NDWI_{GAO}$ before minimum $NDWI_{GAO}$ of 2$^{nd}$ year |
| RF | Re-Flooding | Management: Optional re-flooding of fields during the fallow season. | Inflection point of $NDWI_{GAO}$ after M and before EF. |
| VP | Vegetative Phase | Phenological phase: From germination to panicle initiation | Period between F and T |
| RP | Reproductive Phase | Phenological phase: From panicle initiation, till flowering | Period between T and HD |
| MRP | Maturity-Ripening Phase | Phenological phase: From flowering and ripening till M | Period between HD and M |
| PF | Permanent Flooding | Management: Fields are always flooded but level of water may vary due to punctual drainages. | Period between F and EF. |
| DLP | Dry Land Preparation | Management: rice fields are dry and land is being prepared | Period between EF and F. Related to minimum $NDWI_{GAO}$ and maximum BSI |

For scenario 'D', Pearson's correlation coefficient (*r*) was used for assessing the relationship with available ground truth data of i) Sowing date and $NDWI_{GAO}$-derived flooding (F), ii) Harvest date and NDVI-derived maturity (M) and, iii) Annual rice production (kg·ha$^{-1}$) and the value of the four SI at all dates within the study period.

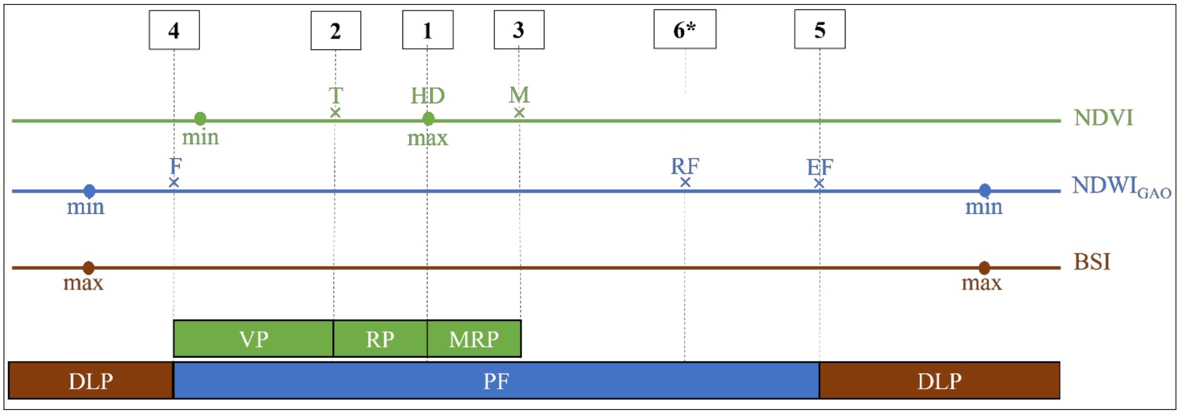


**Figure 4.** Extraction scheme of phenology and irrigation management practices from combined NDVI and $NDWI_{GAO}$ dynamics. Numbers stand for the order of identification of key features, × Inflection Points, ● Local Points. . List of acronyms in Table 2.

# 3. Results

## 3.1. Cloud and shadow masking

We did not conduct a systematic validation of cloud and shadows masking, but it was visually observed that the adaptation of the Schmitt et al. (2019) method improved the default Quality Assessment (QA) cloud mask of S2 L2A imagery (QA60 band), particularly in the presence of disperse or patched clouds (Fig. 5). However, in this situation, problems related to the detection of smallest, thinner clouds and shadows were also observed. These limitations were not addressed from an image processing perspective. In such cases (*e.g.* Fig. 5), the study relied on second filtering (80% of valid pixels within each scenario which include only pixels covering rice paddies), the averaging of pixels and the smoothing of the time series to decrease the impact from the misclassification of clouds and shadows. Overall, 53 of 138 images (ca. 38.5 %) had more than 20 % of pixels affected by clouds or shadows and were discarded; most of them within the period October-December, after the rice growing cycle (Fig. 3).

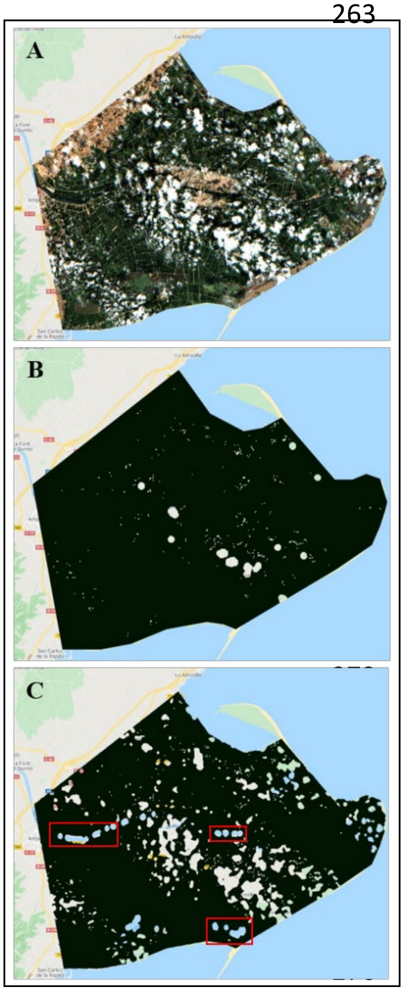


**Figure 5.** The S2 BOA Image clipped to the area of study on 30th July 2019 as viewed in GEE. A) RGB, B) QA60 band-based method, C) Adapted method. Black pixels correspond to not-masked areas. Red squares: Examples of possible overestimation of shadows over water.

## 3.2. Spectral indices time series

The cubic spline smoothing filled gaps for fitting time series with daily information of each spectral index derived from S2 imagery at different scenarios scales. The metrics of the spline fitting (*i.e.* Pearson's *r* and Root Mean Squared Error, *RMSE*), and thus the relationship between observed (*i.e.* satellite-derived) and predicted values, differed among SI. Considering all the scenarios, the weaker correlations were found for $NDWI_{GAO}$ (0.77 <

$r < 0.94$, $0.12 > RMSE > 0.05$), and the strongest correlations were for BSI ($0.84 < r < 0.98$, $0.073 > RMSE > 0.032$), NDWI$_{MF}$ ($0.93 < r < 0.99$, $0.08 > RMSE > 0.04$), and NDVI ($0.95 < \mathrm{r} < 0.99$, $0.09 > \mathrm{RMSE} > 0.04$). These differences were particularly evident during the rice-growing season, and particularly, the variability of NDWI$_{GAO}$ at the beginning of the growing season was not totally retained by the smoothing (Fig. 6C).

At spatial scale, the number of valid images was lower for smaller scenarios (*i.e.* scenario 'D'), and at temporal scale, the number of available images was lower during the post-harvest season, in the autumn-winter period (Fig. 3 and Fig. 6), thus affecting the accuracy of the smoothing. To reduce the uncertainty in these extremes of the smoothed time series, the phenology and hydroperiod phases (see section 3.3) were only classified from the 2018 flooding to the 2019 mature-ripening stage, excluding the initial pre-flooding and final post-harvest periods (Fig. 7). SI showed common patterns among the different scenarios considered, and significant differences were not observed among Scenarios 'A', 'B' and 'C'. Scenario 'D' showed higher variability, mainly due to differences among individual paddy fields, but with common characteristics among them (Fig. 7).

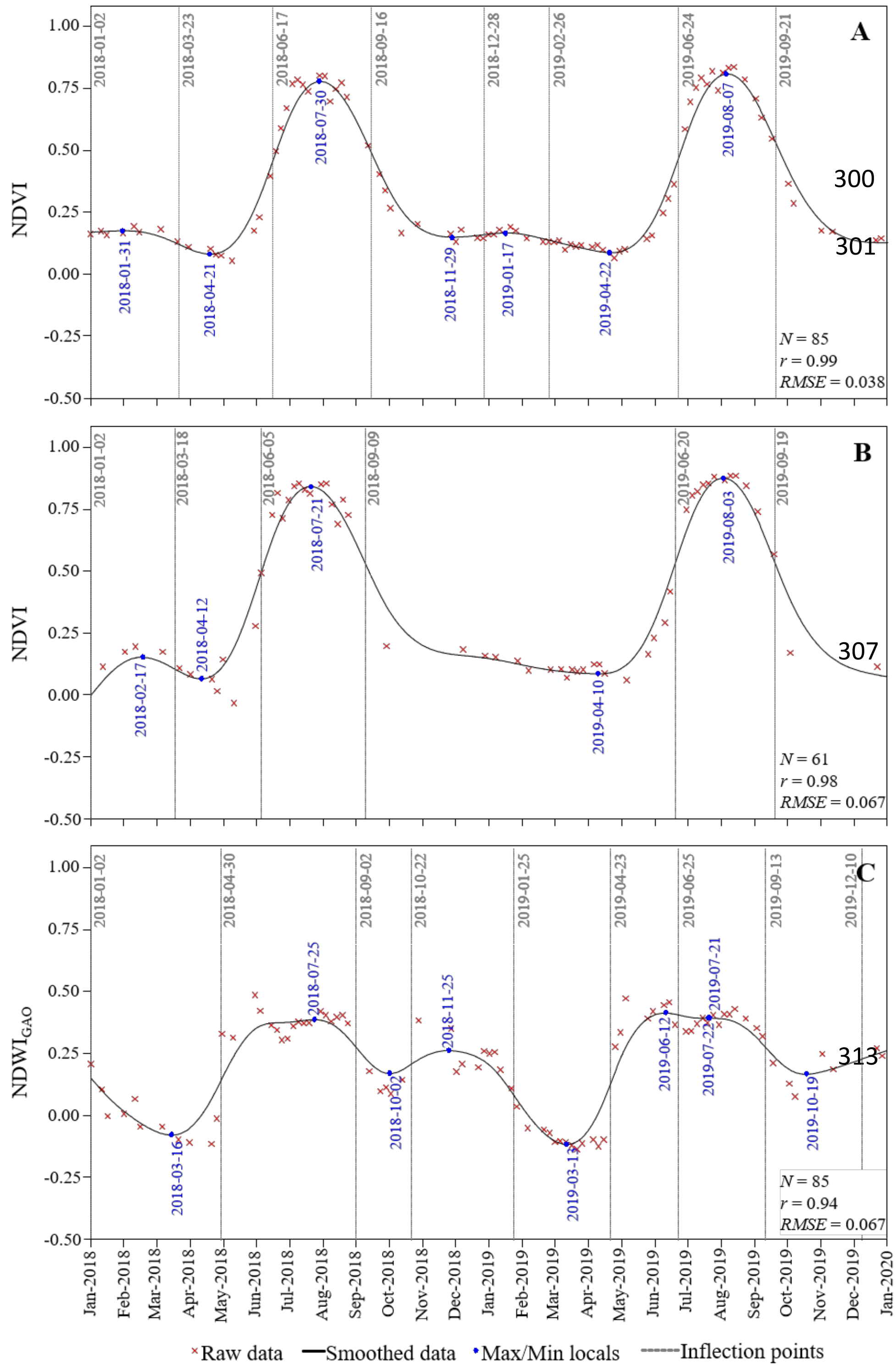


**Figure 6.** Spline smoothing of SI at different spatial scales. A) Mean NDVI in Scenario 'A'; B) Mean NDVI in Field I of Scenario 'D'; C) Mean $NDWI_{GAO}$ in Scenario 'A'. Root Mean Squared Error (RMSE), number of data points (N) and Pearson's r are provided.

Overall, both NDVI and $NDWI_{GAO}$ minimum values were observed between the winter and the middle-spring period, coinciding with maximum BSI. The maximum rate of increase of $NDWI_{GAO}$, associated with flooding, occurred around April-May. Along the growing season, the NDVI reached its maximum in July-August, with the BSI showing an inverse pattern (Fig. 7). After the growing season (autumn and winter) the differences among fields (Scenario 'D') were more evident, and three main SI trends were found: NDVI stabilization with an increase in $NDWI_{GAO}$ and a decrease in BSI; a reduction in both NDVI and $NDWI_{GAO}$ (Field I) with BSI increasing (Fig. 7A); and an increase in both NDVI and $NDWI_{GAO}$ (Field II) associated to a marked decrease in BSI (Fig. 7B).

### 3.3. Phenology and hydroperiod detection

A selection of maximum/minimum and inflection points in NDVI and $NDWI_{GAO}$ time series were used to extract phenology and hydroperiod dynamics for the different scenarios considered (Table 2 and Fig. 4). Flooding (F), active Tillering (T), Heading Date (HD), Maturity (M), End of Flooding (EF), Vegetative Phase (VP), Reproductive Phase (RP), Mature-Ripening Phase (MRP), Permanent Flooding (PF), Re-Flooding (RF), Dry Land and Land Preparation (DLP) crop phases were identified. Comparing the global trends in 2018 and 2019 at different scenarios scales, HD was delayed in 2019 and MRP was shorter in 2019. The temporal variation of NDVI and $NDWI_{GAO}$ indexes were more related to factors such as water management, type of sowing, field characteristics or climate, than to rice cultivar. See for instance Field II (Fig. 7B), where different rice cultivars were sowed in 2018 and 2019.

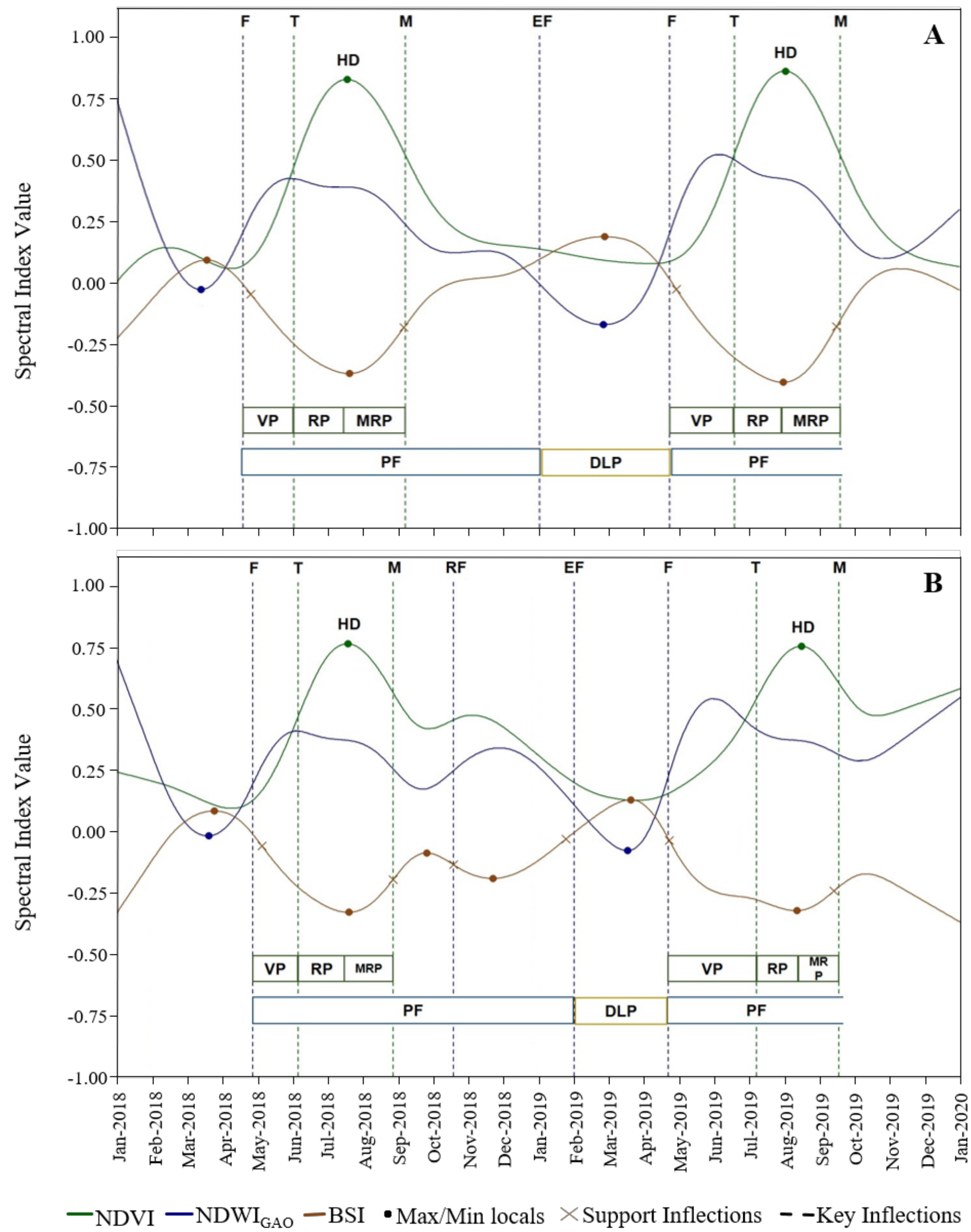


**Figure 7.** Rice phenology and hydroperiod at two different sub-scenarios in the Ebro Delta derived from NDVI and $NDWI_{GAO}$. The BSI trend is shown as supporting information. A) Field I; B) Field II (Fig.1).

The consistency of the results was achieved when only fields with more than 40 valid Sentinel-2 images (during the two years) were included in the analysis (Table 3). On average, Flooding was detected 9 and 12 days before the ground truth sowing date (late

April to late May), and Maturity was observed 6 and 8 days before the ground truth harvest date (late August to early October), in 2018 and 2019 respectively. Despite the larger variability observed between flooding and sowing occurrence, the relationship was > 0.6 (Pearson's *r*) for all evaluated fields with more than 40 Sentinel-2 images (Table 3).

**Table 3**. Relationship between estimated flooding date (F) and ground truth sowing and between estimated maturity date (M) and ground truth harvest data by year. Only fields with more than 40 valid Sentinel-2 images were included.

| Year | $N_{images}$ (min-max) | Key feature | Ground data | $N_{fields}$ | Mean difference (days) | Standard deviation (days) | *r* |
|---|---|---|---|---|---|---|---|
| **2018** | 60 - 82 | Flooding | Sowing | 19 | -12.26 | 3.57 | 0.79 |
| **2018** | 60 - 82 | Maturity | Harvest | 19 | -8.37 | 7.75 | 0.61 |
| **2019** | 41 - 82 | Flooding | Sowing | 23 | -9.04 | 11.68 | 0.66 |
| **2019** | 41 - 82 | Maturity | Harvest | 23 | -6.57 | 3.42 | 0.93 |

## 3.4. Rice yield estimates

In Scenario 'D', SI were correlated (Pearson's *r*) with yield production ($kg{\cdot}ha^{-1}$). The strongest correlations were found in the growing season, mainly between July and middle-August (Fig. 8), with rice yield significantly correlated with all SI. The best correlations observed in 2018 and 2019, respectively, were $r = 0.69$ and $r = 0.74$ with NDVI, 0.82 and 0.66 with $NDWI_{GAO}$, -0.84 and -0.86 with $NDWI_{MF}$, and -0.81 and -0.71 with BSI. Along the summer season, the most consistent relationships with yield production were obtained with $NDWI_{MF}$ and NDVI (Fig. 8).

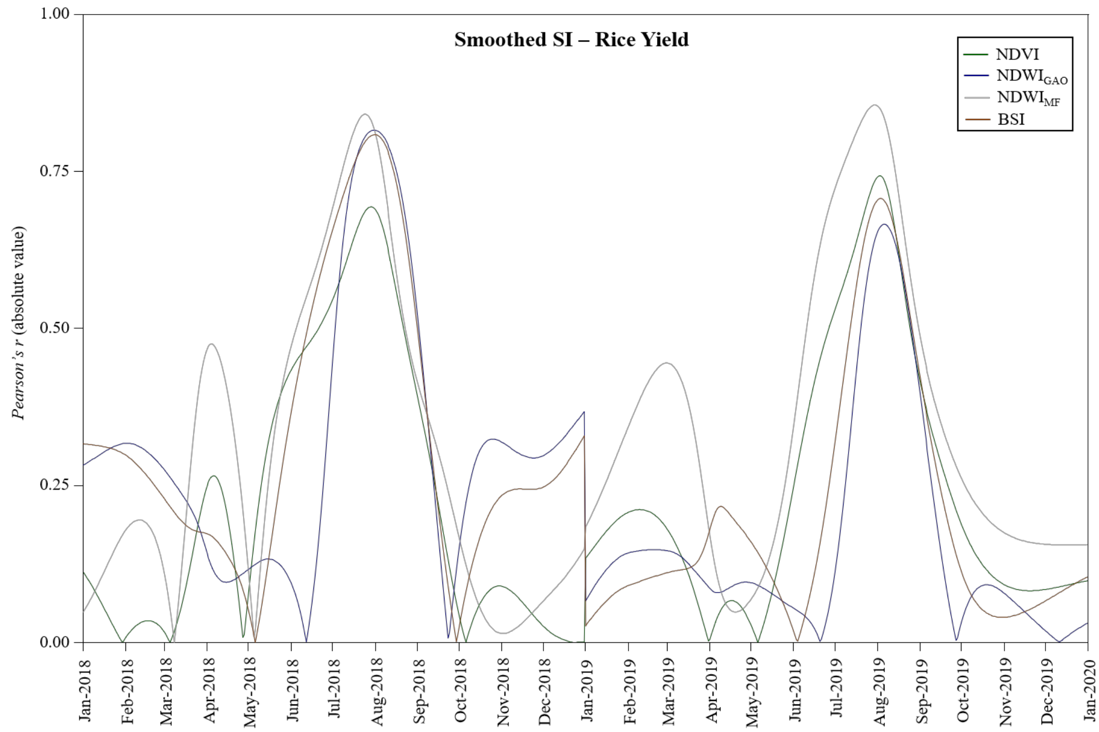


**Figure 8.** Absolute Pearson's correlation (*r*) between parcels production (Kg·ha-1) and SI daily values along the period studied.

For this reason, the study focused on the relationships between rice yield and the annual NDVI maximum (at the HD), and the annual $NDWI_{MF}$ minimum (closest local point to HD). Best results (Fig. 9) were obtained when considering only rice fields with mean NDVI > 0.4 ($r$ = 0.72) or $NDWI_{MF}$ < -0.4 ($r$ = -0.80).

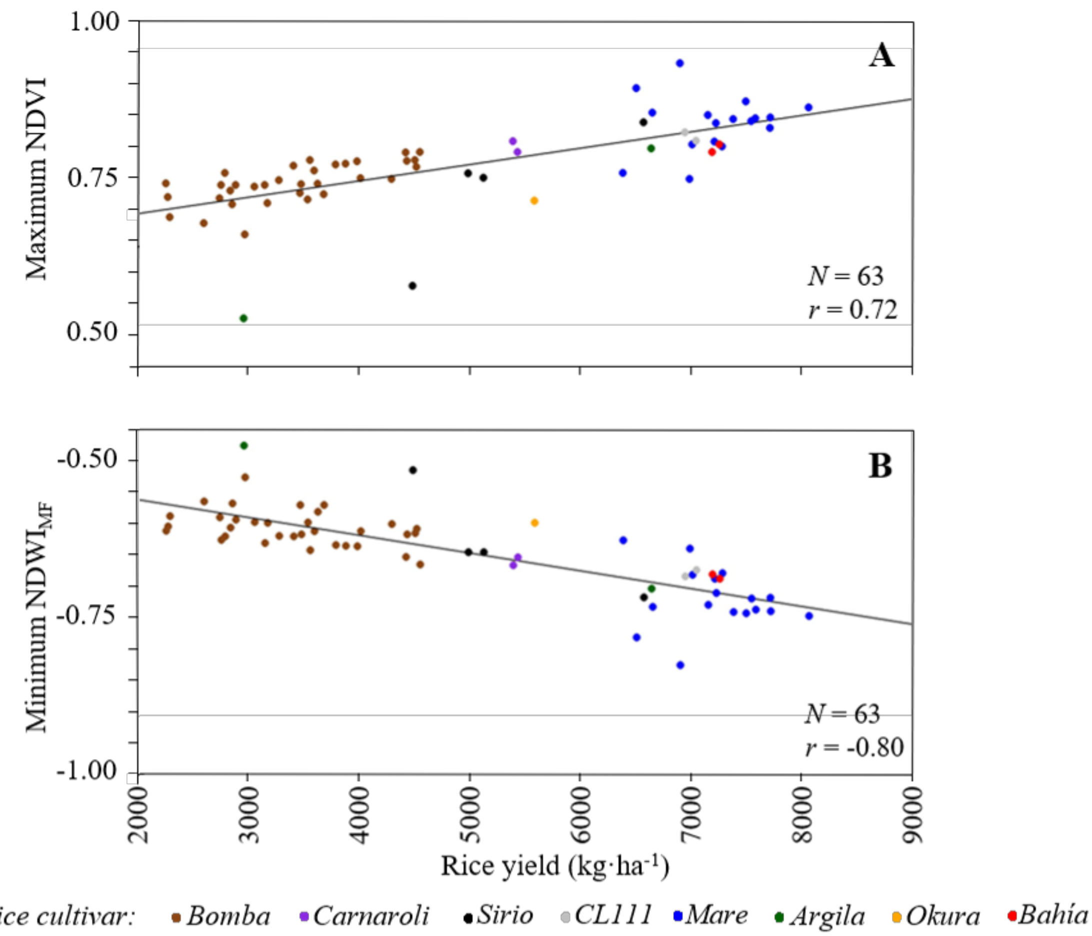


Figure 9. Scatter plot and Pearson's correlation (r) between yearly production by sub-scenarios in 'D' and; A) Maximum yearly NDVI for the corresponding parcels; B) Minimum yearly NDWI$_{MF}$ for the corresponding parcels.

## 4. Discussion

### 4.1. Methodological requirements and limitations

The study has been conducted on a small homogeneous area were rice is the dominant crop. Cadastral information is annually updated from farmers' official declarations. Furthermore, for the assessment on individual fields (Scenario 'D'), ground truth data included yearly information of rice parcels, with single cultivar and crop management in each one. These information were used to conduct a retrospective analysis based on a ‘unit’ approach (pixels averaged within fields under the same conditions) in a single-season and low-yielding system. The proposed methodology has not been tested in other types of rice systems and it is not intended for near real-time monitoring. Additional land cover classification is needed in absence of ancillary data, with particular importance under mixed crops scenarios, thus moving from ‘unit-field’ to ‘pixel-based’ approach and using, for instance, classification methods based on the detection of the particular practice of field flooding, for differentiating rice-growing areas/pixels (Boschetti et al., 2014 and Boschetti et al., 2017). These, may be later aggregated by means of different criteria such as proximity (distance between pixels) or spectral trends’ similarity.

In this study, the main limitation were satellite data gaps since 40 % of the available S2 images for the selected orbit and period had less than 80 % of valid pixels. The number of rejected images increased in smaller scenarios. Although the selection criterion discarded a large number of S2 images, it was necessary for reducing the uncertainty related to cloud and cloud shadow miss-detection and reducing the noise of final mean SI values. Cloud presence and cloud shadow masking is a key issue in optical remote sensing, and the default operational Sentinel-2 QA60 has been shown to commit high errors in presence of thin or patched clouds (Coluzzi *et al.*, 2018). Thus, we preferred the adapted masking method of Schmitt et al. (2019), which has the advantage that can be easily tuned, making it suitable for a wide range of scenarios. The mean gap between consecutive images was 9 days, usually ranging between 5 (S2 temporal resolution) and 10 days, thus improving other similar platforms such as Landsat, with a best temporal resolution of 16 days. The largest gaps due to cloud presence were of 25 days (November 2019), 30 days (November 2018), and 40 days (December 2019), but in these months a lower variability in rice fields is expected (the growing season is from mid-April to early September) and a reduced temporal resolution during this period did not affect the results significantly. Increasing temporal resolution is more important in the growing season when changes occur within days or weeks. In this case, further research should consider improving the methodology for thin cloud and clouds shadows masking for reducing data gaps, particularly, at field scale. Although it can provide valuable information, our results indicate that Sentinel-2 alone is not enough for an accurate phenology monitoring for crop management. In this sense, it is suggested the use of multi-platform data. In the optical domain, the fusion of Sentinel-2 and Landsat-8 is recommended (Liu et al., 2020, Boschetti et al., 2018), since both platforms' pixel sizes are smaller than individual rice fields. A complementary approach is generating cloud-free time series of synthetic high-resolution images (*e.g.* Sentinel-2, Landsat-7/8) from moderate resolution data such as MODIS imagery (Wu et al., 2018, Gao *et al*., 2015). However, image processing of data from multiple satellites/sensors is challenging, for instance, due to differences in their orbital, spatial, spectral response functions, and image processing chains (Campos-Taberner *et al*., 2017).

### 4.2. Application of spectral indices

The NDVI and $NDWI_{GAO}$ were combined to estimate key cropping phases (*i.e.* Flooding, Tillering, Harvest, Maturity, and Re-Flooding), and $NDWI_{MF}$ was related to crop yield. NDVI was limited to the rice-growing season for assessing rice phenology, mainly Tillering, Heading Date, and Maturity. In previous studies, NDVI has been used for showing the transition from bare flooded soil to rice emergence (Tornos *et al.*, 2015). In this study, this transition was not clearly identified since the canopy cover is scarce at the beginning of the cropping and soil-related factors may affect NDVI values (Zhang *et al.*, 2019). In relation to the identification of the Tillering stage, the temporal gap between Flooding and Tillering agreed with the common rice farming calendar in the Ebro Delta (Fig. 2). Although the proposed method differentiated small variability between nearby fields' dynamics (Scenario 'D'), no phenological field data were available for validating its accuracy. We used the NDVI inflection point before the Heading Date for defining the start of the active Tillering stage as previous works have reported that active Tillering is associated with the maximum increase rate of NDVI, related to the fast growth of rice plants during this stage (Zheng *et al*., 2016). The Heading Date has been related to the maximum in NDVI, which is associated to a peak in Leaf Area Index (LAI), showing an increase in plant biomass (Wang *et al*., 2014). The maturity date (M) is associated with a rapid decrease of NDVI at the end of this stage (Zheng et al., 2016) and it was significantly related to the harvest date ($r > 0.6$). The delay observed between the maturity date (S2-derived) and the harvest date (reference data) could be related to farmers' harvest practices, since harvest is mediated not only because the ripening state of rice but also considers other external factors (*e.g.* weather, machinery availability).  However, more ground truth data including also additional information (*e.g.* HD, T) and covering a larger extension (ground truth data in this study was limited to a subset of spatially aggregated fields) is further needed for deeply assessing the accuracy on the identification of key phenology features through the proposed extraction scheme. $NDWI_{GAO}$ variations were associated with hydroperiod and can be applied as an indicator of flooding management in rice paddies (*i.e.* Flooding, End of Flooding and Re-Flooding). Our results were similar to those reported in Tornos *et al*. (2015) in the Ebro Delta and Boschetti *et al.* (2014) in rice fields from Italy, both using data derived from MODIS. The $NDWI_{GAO}$ responds to water level fluctuations from flooding to rice tillering, and after the rice is harvested. However, with the increase in leaf coverage during the reproductive and rice ripening phases, $NDWI_{GAO}$ could be more associated with the canopy structure and mediated by plant water content and metabolic activity (Zhang *et al.*, 2019; Serrano *et al*., 2019). For the same reason, the identified Re-flooding (RF) should be carefully considered in presence of a second NDVI peak after harvest (*e.g.* Fig.7B). This peak may be related to the presence of weed or rice regrowth (Tornos *et al.* 2015) with an expected impact on the $NDWI_{GAO}$ dynamics. Consequently, $NDWI_{GAO}$ is useful for complementing NDVI-derived phenology and vegetation status in rice fields, but the index variability increases in the presence of vegetation, highlighting the need to improve data frequency. The $NDWI_{GAO}$ derived flooding results are a promising estimator of the sowing date ($r > 0.6$), with sowing occurring, on average, 9 to 12 days after flooding (Table 3). Despite these differences are in agreement with the general rice farming calendar in the Ebro Delta (Fig. 2), high variability was observed (up to ±11 days). This variability may be explained by different types of sowing (*e.g.* direct seeding, transplanting, dry-seeding) and farmer's decisions on sowing time, which increase the uncertainty in their relationship. These issues must be further tackled, but ground truth data regarding water management practices and sowing management are needed.

The BSI was mainly used as a reference for complementing the analysis on NDVI and $NDWI_{GAO}$ results, under the assumption that maximum BSI occurs when a rice field has no water and no vegetation. Applying the first and second derivatives analysis on BSI showed that minimum and maximum were related with HD and dry land, respectively; while inflection points in BSI were closer to the identified flooding and maturity-harvest (Fig. 7). A further assessment of BSI capabilities within the proposed extraction scheme is planned, since it may combine important key features of both NDVI and $NDWI_{GAO}$ for the management of rice-growing areas.

Finally, $NDWI_{MF}$ temporal pattern was similar but inverse to NDVI, thus no additional information on crop cycle was obtained. However, minimum $NDWI_{MF}$ was highly correlated to crop yield in the Ebro Delta ($r$ = -0.80), showing good agreement between fields with different yields and cultivars (Fig. 9). $NDWI_{MF}$ includes the same spectral bands as the Green NDVI (Gitelson *et al*., 1996) which has been used before for crop yield estimates (Moreno-García *et al.*, 2018). In low-yielding rice s (< 9000 $Kg{\cdot}ha^{-1}$), such as the Ebro Delta, two spectral bands SI are not affected by the saturation phenomenon due to low crop biomass (Xue *et al.*, 2014), thus explaining the strong relationship observed between $NDWI_{MF}$ and yield. Different from the relationship achieved for sowing and harvest, crop yield estimates were not strictly related to the number of valid satellite images of the study period. It is explained because the minimum $NDWI_{MF}$ used occurs close to the HD, in summer, when smaller data gaps are expected. Nevertheless, previous studies have n that from tillering to harvest, different stages of rice are suitable for crop yield estimation (Xue *et al.*, 2014; Cao *et al.*, 2016; Moreno-García *et al.*, 2018), but these stages can be more complex to identify.

### 4.3. Ebro Delta Rice Development (2018-2019) and Management Implications

In terms of rice paddies dynamics, similar results were obtained in Scenarios ‘A’, ‘B’, ‘C’, and in most of the fields in Scenario ‘D’, thus showing the homogeneity of agricultural practices in the Ebro Delta along the study period (2018-2019). Those results are similar to those reported by Tornos *et al.* (2015) from 2001 to 2012, which suggested not only spatial but also temporal homogeneity in rice management in the Ebro Delta. Considering Scenarios ‘A’, ‘B’ and ‘C’, the main differences between both years related to rice development were a delay in heading date and a larger ripening phase in 2019, which might be mediated by climatologic factors. For instance, before the start of the growing season, the total precipitation in April varied between 40.5 mm in 2018 to 8.9 mm in 2019 (Meteorological Service of Catalonia, https://www.meteo.cat/wpweb/climatologia). Although different meteorological factors (*e.g.* air, solar radiation) or soil features may affect the crop (Sánchez *et al*., 2013; Zhao *et al.*, 2016), heavy rains increase fields' water level, which mitigates heat and salinity stress to the crop (Martínez-Eixarch *et al.*, 2018), contributing to modulate the length of the different phenological phases of the crop. At small spatial scales, our study provides an insight into the potential of S2-derived SI for the characterization and assessment of the dynamics of rice fields and crop yield estimates in low-yielding rice farming systems. The proposed method allowed to capture small dynamics variations among fields (Scenario 'D'), automatically, with importance from a management/planning sight. For instance, yearly crop yield estimates at field-level or different field management practices after harvest (*e.g.* re-flooding, progressive drying or rice regrowth) are key aspects for the development of agro-environmental policies and productive and sustainable wetlands. Further research will focus on increasing both satellite and ground truth data for addressing the main limitations found and being able to provide relevant information for authorities at a regional scale.

## 5. CONCLUSIONS

Atmospheric conditions (*e.g.* cloud presence) and differences in rice fields characteristics (*e.g.* area, soil properties, management practices) increase the difficulty of using coarse resolution or low-frequency multispectral satellite data (*e.g* MODIS, Landsat) for the effective monitoring of agricultural practices and crop efficiency. For these purposes, in this study, we used three different spectral indexes (NDVI, $NDWI_{MF}$, $NDWI_{GAO}$) from

Sentinel-2 (temporal frequency of 5 days). At different spatial scales, key rice farming features were identified (*i.e.* Flooding, Tillering, Heading Date, Maturity, End of Flooding and Re-Flooding after harvest), thus defining the main phenological phases of the crops (*i.e.* Vegetative Phase, Reproductive Phase, Maturity-Ripening Phase), identifying flooding regimes (flooded or dry), and producing accurate estimates of rice yield. However, few ground truth data were available and, satellite data gaps due to cloud cover limited significantly the applicability of the method at smaller spatial scales, restricting its capabilities in several fields. Further research must address these issues by increasing the density of satellite data (*e.g.* multi-platform data, enhanced cloud and shadows masking) and reference data for fully assessing the accuracy of the proposed key features' extraction scheme and its extended applicability to all the Ebro Delta region and other similar areas (deltaic low-yielding rice systems).

**Acknowledgements**

Jesús Soriano held a pre-doctoral grant funded by Agència de Gestió d'Ajuts Universitaris i de Recerca (2020 FI B200148). Authors also acknowledge support from CERCA Programme (Generalitat de Catalunya). The authors are especially grateful to Joan Trias for providing reference data and collaboration.

## References

Bolton, D.K., Gray, J.M., Melaas, E.K., Moon, M., Eklundh, L. and Friedl, M.A. 2020. "Continental-scale land surface phenology from harmonized Landsat 8 and Sentinel-2 imagery." Remote Sensing of Environment 240, 111685. https://doi.org/10.1016/j.rse.2020.111685.

Boschetti, M., Nutini, F., Manfron, G., Brivio, A., and Nelson, A. 2014. “Comparative Analysis of Normalised Difference Spectral Indices Derived from MODIS for Detecting Surface Water in Flooded Rice Cropping Systems.” PLoS ONE 9 (2): e88741. https://doi.org/10.1371/journal.pone.0088741.

Boschetti, M., Busetto, L., Manfron, G., Laborte, A., Asilo, S., Pazhanivelan, S., and Nelson, A. 2017. “PhenoRice: A method for automatic extraction of spatio-temporal information on rice crops using satellite data time series”. Remote Sensing of Environment 194: 347-365.

Boschetti, M., Busetto, L., Ranghetti, L., Garcia-Haro, J., Campos-Taberner, M., and Confalonieri, R. 2018. "Testing Multi-Sensors Time Series of Lai Estimates to Monitor Rice Phenology: Preliminary Results," In IGARSS 2018 - 2018 IEEE International Geoscience and Remote Sensing Symposium, 2018, pp. 8221-8224, doi: 10.1109/IGARSS.2018.8518494.

Bradley, B.A., Jacob, R.W., Hermance, J.F., and Mustard, J.F. 2007. “A Curve Fitting Procedure to Derive Inter-Annual Phenologies from Time Series of Noisy Satellite NDVI Data.” Remote Sensing of Environment 106 (2): 137–45. https://doi.org/10.1016/j.rse.2006.08.002.

Campos-Taberner, M., García-Haro, F.J., Camps-Valls, G., Grau-Muedra, G., Nutini, F., Busetto, L., Katsantonis, D., Stavrakoudis, D., Minakou, C., Gatti, L., Barbieri, M., Holecz, F., Stroppiana, D., and Boschetti, M. 2017. “Exploitation of SAR and Optical Sentinel Data to Detect Rice Crop and Estimate Seasonal Dynamics of Leaf Area Index”. Remote Sensing 9 (3).

Cao, Q., Jianning, Y.M., Yu, S.W., Yuan, F., Cheng, S., Huang, S., Wang, H., Yang, W., and Liu, F. 2016. “Improving In-Season Estimation of Rice Yield Potential and Responsiveness to Topdressing Nitrogen Application with Crop Circle Active Crop Canopy Sensor.” Precision Agric 17: 136–54. https://doi.org/10.1007/s11119-015-9412-y.

Casanova, D. 1998. “Quantifying the Effects of Land Conditions on Rice Growth. A Case Study in the Ebro Delta (Spain) Using Remote Sensing.” Wageningen University, The Netherlands.

Coluzzi, R., Imbrenda, V., Lanfredi, M., and Simoniello, T. 2018. “A First Assessment of the Sentinel-2 Level 1-C Cloud Mask Product to Support Informed Surface Analyses.” Remote Sensing of Environment 217 (August): 426–43. https://doi.org/10.1016/j.rse.2018.08.009.

Courault, D., Hossard, L., Flamain, F., Baghdadi, N., and Irfan, K. 2020. “Assessment of agricultural practices from Sentinel 1 and 2 images applied on rice fields to develop a farm typology in the Camargue region.” In IEEE Journal of Selected Topics in Applied Earth Observations and Remote Sensing 13: 5027-5035. https://doi.org/10.1109/JSTARS.2020.3018881.

Dong, J., and Xiao, X. 2016. “Evolution of Regional to Global Paddy Rice Mapping Methods: A Review.” ISPRS Journal of Photogrammetry and Remote Sensing 119: 214–27. https://doi.org/10.1016/j.isprsjprs.2016.05.010.

Fernandez-Beltran, R., Baidar, T., Kang, J. and Pla, F. 2021. “Rice-Yield Prediction with Multi-Temporal Sentinel-2 Data and 3D CNN: A Case Study in Nepal.” Remote Sensing 13, 1391. https://doi.org/10.3390/rs13071391

Gao, B-C. 1996. “NDWI - A Normalized Difference Water Index for Remote Sensing of Vegetation Liquid Water from Space.” Remote Sensing of Environment 7212 (April): 257–66.

Gao, F., Hilker, T., Zhu, X., Anderson, M., Masek, J., Wang, P., and Yang, Y. 2015. "Fusing Landsat and MODIS Data for Vegetation Monitoring," in IEEE Geoscience and Remote Sensing Magazine, 3 (3): 47-60. doi: 10.1109/MGRS.2015.2434351.

Geng, L., Ma, M., Wang, X., Yu, W., Jia, S., and Wang, H. 2014. “Comparison of Eight Techniques for Reconstructing Multi-Satellite Sensor Time-Series NDVI Data Sets in the Heihe River Basin, China.” Remote Sensing 6 (3): 2024–49. https://doi.org/10.3390/rs6032024.

Genua-Olmedo, A., Alcaraz, C., Caiola, N., and Ibáñez, C. 2016. “Sea Level Rise Impacts on Rice Production: The Ebro Delta as an Example.” Science of the Total Environment 571: 1200–1210. https://doi.org/10.1016/j.scitotenv.2016.07.136.

Gitelson, A.A., Kaufman, Y.J., and Merzlyak, M.N. 1996. “Use of Green Channel in Remote Sensing of Global Vegetation from EOS-MODIS.” Remote Sensing of Environment 58 (3): 289–98. https://doi.org/10.1016/S0034-4257(96)00072-7.

Gorelick, N., Hancher, N., Dixon, M., Ilyushchenko, S., Thau, D., and Moore, R. 2017. “Google Earth Engine: Planetary-Scale Geospatial Analysis for Everyone.” Remote Sensing of Environment 202: 18–27. https://doi.org/10.1016/j.rse.2017.06.031.

Liu, S., Liu, X., Liu, M., Wu, L., Ding, C., and Huang, Z. 2017. “Extraction of rice phenological differences under heavy metal stress using EVI time-series from HJ-1A/B data”. Sensors (Switzerland) **17**, 1–17.

Liu, L., Xiao, X., Qin, Y., Wang, J., Xu, X., Hu, Y. and Qiao, Z. 2020. “Mapping cropping intensity in China using time series Landsat and Sentinel-2 images and Google Earth Engine”. Remote Sensing of Environment 239, 111624.

Martínez-Eixarch, M., Curcó A. and Ibañez, C. 2016. “Effects of agri-environmental and organic rice farming on yield and macrophyte community in Mediterranean paddy fields”. Paddy Water Environment 15: 457-468. https://doi.org/10.1007/s10333-016-0563-x.

Martínez-Eixarch, M., Alcaraz, C., Viñas, M., Noguerol, J., Aranda, X., Prenafeta-Boldu, F.X., Saldaña-De la Vega, J.A., Catala, M.M., and Ibañez, C. 2018. “Neglecting the Fallow

Season Can Significantly Underestimate Annual Methane Emissions in Mediterranean Rice Fields." PLoS ONE 13. https://doi.org/10.1371/journal.pone.0198081.

McFeeters, S.K. 1996. "The Use of the Normalized Difference Water Index (NDWI) in the Delineation of Open Water Features." International Journal of Remote Sensing 17 (7): 1425–32. https://doi.org/10.1080/01431169608948714.

Misra, G., Cawkwell, F., and Wingler, A. 2020. "Status of Phenological Research Using Sentinel-2 Data: A Review." Remote Sensing 12 (17): 10–14. https://doi.org/10.3390/RS12172760.

Moreno-García, B., Casterad, M.A., Guillén, M., and Quílez, D. 2018. "Agronomic and Economic Potential of Vegetation Indices for Rice N Recommendations under Organic and Mineral Fertilization in Mediterranean Regions." Remote Sensing 10 (12). https://doi.org/10.3390/rs10121908.

Mosleh, M.K., Hassan, Q.K., and Chowdhury, E.H. 2015. "Application of Remote Sensors in Mapping Rice Area and Forecasting Its Production: A Review." Sensors (Switzerland) 15 (1): 769–91. https://doi.org/10.3390/s150100769.

RCoreTeam. 2017. "R: A Language and Environment for Statistical Computing." Vienna, Austria: R Foundation for Statistical Computing.

Rikimaru, A., Roy, P. S., and Miyatake, S. 2002. "Tropical Forest Cover Density Mapping." Tropical Ecology 43 (1): 39–47.

Rouse, J.W., Haas, R.H., Schell, J.A., and Deering, D.W. 1974. "Monitoring Vegetation Systems in the Great Plains with ETRS." In Third Earth Resources Technology Satellite-1 Symposium, 309–17. Washington DC: Goddard Space Flight Center, NASA SP-351, Science and Technical Information office, NASA.

Sakamoto, T., Yokozawa, M., Toritani, H., Shibayama, M., Ishitsuka, N., and Ohno, H. 2005. "A Crop Phenology Detection Method Using Time-Series MODIS Data." Remote Sensing of Environment 96 (3–4): 366–74. https://doi.org/10.1016/j.rse.2005.03.008.

Sánchez, B., Rasmussen, A., and Porter, J.R. 2013. "Temperatures and the Growth and Development of Maize and Rice: A Review." Global Change Biology 20 (2): 408–17. https://doi.org/10.1111/gcb.12389.

Schmitt, M., Hughes, L. H. , Qiu, C., and Zhu, X. X. 2019. "Aggregating Cloud-Free Sentinel-2 Images With Google Earth Engine." ISPRS Annals of Photogrammetry, Remote Sensing and Spatial Information Sciences IV-2/W7 (December): 145–52. https://doi.org/10.5194/isprs-annals-iv-2-w7-145-2019.

Serrano, J., Shahidian, S., and Da Silva, J.M. 2019. "Evaluation of Normalized Difference Water Index as a Tool for Monitoring Pasture Seasonal and Inter-Annual Variability in a Mediterranean Agro-Silvo-Pastoral System." Water (Switzerland) 11 (1). https://doi.org/10.3390/w11010062.

Tornos, L., Huesca, M., Dominguez, J.A., Moyano, M.A, Cicuendez, V., Recuero, L., and Palacios-Orueta, A. 2015. “Assessment of MODIS Spectral Indices for Determining Rice Paddy Agricultural Practices and Hydroperiod.” ISPRS Journal of Photogrammetry and Remote Sensing 101: 110–24. https://doi.org/10.1016/j.isprsjprs.2014.12.006.

Wan, L., Cen, H., Zhu, J., Zhang, J., Zhu, Y., Sun, D., Du, X., Zhai, L., Weng, H., Li, Y., Li, X., Bao, Y., Shou, J., and He, Y. 2020. “Grain Yield Prediction of Rice Using Multi-Temporal UAV-Based RGB and Multispectral Images and Model Transfer – a Case Study of Small Farmlands in the South of China.” Agricultural and Forest Meteorology 291 (March): 108096. https://doi.org/10.1016/j.agrformet.2020.108096.

Wang, H., Chen, J., Wu, Z., and Lin, H. 2012. “Rice Heading Date Retrieval Based on Multi-Temporal MODIS Data and Polynomial Fitting.” International Journal of Remote Sensing 33 (6): 1905–16. https://doi.org/10.1080/01431161.2011.603378.

Wang, L., Zhang, F-C., Jing, Y-S., Jiang, X-D., Yang, S-B., and Han, X-M. 2014. “Multi-Temporal Detection of Rice Phenological Stages Using Canopy Stagespectrum.” Rice Science 21 (2): 108–15. https://doi.org/10.1016/S1672-6308(13)60170-5.

Wang, Y. 2011. Smoothing Splines: Methods and Applications. Edited by F Bunea, V Isham, N Keiding, T Louis, R.L. Smith, and H Tong. Smoothing Splines: Methods and Applications. Santa Barbara, California, USA: CRC Press.

Wu, M., Yang, C., Song, X., Hoffmann, W.C., Huang, W., Niu, Z., Wang, C., Li, W. and Yu, B. 2018. “Monitoring cotton root rot by synthetic Sentinel-2 NDVI time series using improved spatial and temporal data fusion”. Sci Rep 8, 2016. https://doi.org/10.1038/s41598-018-20156-z

Xue, L., Li, G., Qin, X., Yang, L., and Zhang, H. 2014. “Topdressing Nitrogen Recommendation for Early Rice with an Active Sensor in South China.” Precision Agric 15: 95–110. https://doi.org/10.1007/s11119-013-9326-5.

Zheng, H., Cheng, T., Yao, X., Deng, X., Tian, Y., Cao, W., and Zhu, Y. 2016. Detection of rice phenology through time series analysis of ground-based spectral index data. *F. Crop. Res.* **198**, 131–139.

Zeng, L., Wardlow, B.D., Xiang, D., Hu, S., and Li, D. 2020. “A Review of Vegetation Phenological Metrics Extraction Using Time-Series, Multispectral Satellite Data.” Remote Sensing of Environment 237 (October 2019): 111511. https://doi.org/10.1016/j.rse.2019.111511.

Zhang, B., Liu, X., Liu, M., and Meng, Y. 2019. “Detection of Rice Phenological Variations under Heavy Metal Stress by Means of Blended Landsat and MODIS Image Time Series.” Remote Sensing 11 (1). https://doi.org/10.3390/rs11010013.

Zhao, H., Fu, Y.H., Wang, X., Zhao, C., Zeng, Z., and Piao, S. 2016. “Timing of Rice Maturity in China Is Affected More by Transplanting Date than by Climate Change.”

Agricultural and Forest Meteorology 216: 215–20. https://doi.org/10.1016/j.agrformet.2015.11.001.

Zhu, Z., Wulder, M.A., Roy, D.P., Woodcock, C.E., Hansen, M.C., Radeloff, V.C., Healey, S.P., Schaaf, C., Hostert, P., Strobl, P., Pekel, J-F., Lymburner, L., Pahlevan, N., and Scambos, T.A. 2019. “Benefits of the free and open Landsat data policy”. Remote Sensing of Environment 224: 382-385. https://doi.org/10.1016/j.rse.2019.02.016.